Inorganic Chemistry

Article

pubs.acs.org/IC

Liquid-Crystalline Zinc(II) and Iron(II) Alkyltriazoles One-Dimensional Coordination Polymers

Pauline Grondin,[†,‡] Diana Siretanu,[†,‡] Olivier Roubeau,*[,†,‡,§] Marie-France Achard,[†,‡] and Rodolphe Clérac*[,†,‡]

[†]CNRS, CRPP, UPR 8641, F-33600 Pessac, France

[‡]Univ. of Bordeaux, CRPP, UPR 8641, F-33600 Pessac, France

[§]Instituto de Ciencia de Materiales de Aragón (ICMA), CSIC−Universidad de Zaragoza, Departamento de Física de la Materia Condensada, Facultad de Ciencias, Pedro Cerbuna 12, 50009 Zaragoza, Spain

Supporting Information

ABSTRACT: Several series of unidimensional coordination polymers of formula $[Zn(C_nH_{2n+1}trz)_3](Cl)_2{\cdot}xH_2O$ (n = 18, 16, 13, 11, 10, trz = 4-substituted-1,2,4-triazole), $[Zn(C_{18}H_{37}trz)_3](ptol)_2{\cdot}xH_2O$, $[Fe(C_nH_{2n+1}trz)_3](X)_2{\cdot}xH_2O$ (n = 18, 16, 13, 10; X = Cl^- or $ptol^-$, where $ptol^-$ = p-tolylsulfonate anion), and $[Fe(C_{18}H_{37}trz)_3](X)_2{\cdot}xH_2O$ (X = $C_8H_{17}PhSO_3^-$ and $C_8H_{17}SO_3^-$) are reported with their thermal, structural, and magnetic properties. Most of these materials exhibit thermotropic lamellar mesophases at temperatures as low as 410 K, as confirmed by textures observed by polarized optical microscopy. The corresponding phase diagrams deduced by differential scanning calorimetry are also reported. All iron-containing materials present a spin crossover phenomenon that occurs at temperatures ranging from 242 to 360 K, only slightly below the mesophase temperature domain, and remains complete and cooperative, even for the longer alkyl substituents. The use of stable diamagnetic Zn(II) analogues proves to be very useful to characterize the comparatively less stable and less crystalline Fe(II) analogues.

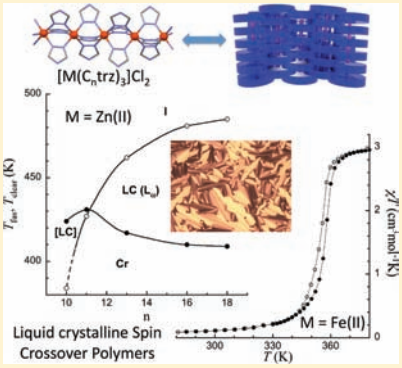

INTRODUCTION

In modern materials science, a large domain of research is devoted to obtain a synergy between two or more physical properties in materials[1] through flexible synthesis of molecular assemblies or formulation. The thermal spin crossover (SC) phenomenon yields a synergetic effect between the magnetic and the optical properties, in particular, in Fe(II) coordination complexes.[2] In certain so-called "cooperative systems", large thermal hysteresis cycles are observed, resulting from elastic network interactions between SC complexes induced by either direct bonding in coordination polymers or supramolecular interactions like H-bonding networks and $\pi-\pi$ stacking.[3] Indeed, SC complexes have been used in a large number of multifunctional materials.[4] Implementing the magnetic and optical bistabilities of SC systems within a liquid crystal (LC) mesophase would, in addition to its intrinsic optical and magnetic properties, allow a different control of the LC orientation by external weak magnetic field depending on the magnetic state of the SC unit (diamagnetic or paramagnetic). This molecular control would bring great advantages within the field of metallomesogens,[5] in particular, for applications of liquid crystals for which the color is necessary. The coexistence of a SC phenomenon and thermotropic LC properties has been demonstrated already a decade ago[6] in a mononuclear Fe(III) complex bearing dodecyloxybenzoyloxy arms. Nevertheless, since the smectic mesophase (T > 391 K) occurred well above the temperature range of the SC of this complex, no synergy between the two existing phenomena was observed. The same conclusion holds for the first SC Fe(II) monomeric complexes exhibiting a thermotropic mesophase.[7] Therefore, researchers orientated their projects toward complexes with higher spin crossover temperatures and a more cooperative phenomenon. In that sense, polymeric one-dimensional triazole-based Fe(II) materials of general formula $[Fe(Rtrz)_3](A)_2{\cdot}xH_2O$ (Rtrz = 4-substituted-1,2,4-triazole; A^- = monovalent anion)[8] are particularly attractive as already illustrated by the elaboration of SC nanoparticles,[9] supramolecular gels,[10] and thin films[11] and development of optical devices prototypes.[12] One of the advantages of these materials is their flexibility. For the $[Fe(Rtrz)_3](A)_2$ system, the SC temperature and cooperative character can be easily tuned by the nature of the 4-substituent on the triazole ligand and/or choice of the A^- counteranion.[13] Indeed, pro-mesogenic bis-alkyloxybenzylformylamino substituents could be introduced within these compounds, yielding a synergic effect between a structural change and the spin crossover, just above room temperature.[14] Nevertheless, no information on the nature of the high-temperature phase was reported, while the observed SC was unfortunately very incomplete. More recently, Gaspar et al. studied series of similar

Received: February 22, 2012
Published: April 9, 2012

   dx.doi.org/10.1021/ic300404r | Inorg. Chem. 2012, 51, 5417−5426

compounds with different counteranions.[15] Columnar or columnar lamellar mesophases were observed for the longer chains with 8, 10, and 12 carbons, but the SC remained gradual and also incomplete, while mesophase textures were actually not reported. Although the use of bulky pro-mesogenic substituents on the triazole ligands is clearly a good strategy to produce materials with coexisting SC and LC properties, maintaining a cooperative and complete SC while favoring a fluid mesophase remains a difficult task.[16]

In order to obtain SC gels and Langmuir−Blodgett films, our research group has been interested in several series of such M(II) triazole-based polymeric materials with long alkyl substituents.[10a,11a,17] These comparatively simpler substituents may still represent a good alternative to tackle the remaining drawbacks of these SC/LC systems. The first important objective of our work is to maintain the typical cooperative behavior of these materials even with pro-mesogenic substitutents. This is not straightforward since even if the one-dimensional structure may possess some intrinsic cooperativity thanks to the direct N1,N2-triazole bridges, isolation of the chains naturally tends toward a solution-like crossover behavior. Moreover, too bulky substituents on the 4 position of the triazoles result in strong shortening of the chain length and thus in incomplete and gradual SC as shown by the bis-alkyloxybenzylformylamino-substituted systems.[14,15] The second important aspect is related to the synchronism in temperature or best to the possible synergetic effects between the spin crossover and the crystal (Cr) to LC transition phenomena. In order to design a material with a SC in the mesophase or a SC simultaneous to or induced by the Cr to LC transition, the SC characteristic temperature, T_{SC}, must be above room temperature. This can be achieved using the right anions such as halides or sulfonates, known to induce SC at such temperatures.[18] Nevertheless, although quite stable, these Fe(II)−triazole compounds tend to undergo oxidation and decomposition at temperatures above 180 °C (453 K). Then, lowering the temperature domain of the mesophase is also an important issue. In this respect, a long alkyl substituent may represent a good compromise. Finally, use of similar systems with other metal ions such as Zn(II) would allow one to perform thermal studies free of potential oxidation/decomposition effects.

We report here on the thermal and structural behavior of the compounds $[Zn(C_nH_{2n+1}trz)_3](Cl)_2{\cdot}xH_2O$ (n = 18, 16, 13, 11, 10), $[Zn(C_{18}H_{37}trz)_3](ptol)_2{\cdot}xH_2O$, and $[Fe(C_nH_{2n+1}trz)_3](X)_2{\cdot}xH_2O$ (n = 18, 16, 13, 10, X = Cl^-, $ptol^-$, where $ptol^-$ = p-tolylsulfonate anion), and $[Fe(C_{18}H_{37}trz)_3](X)_2{\cdot}xH_2O$ (X = $C_8H_{17}SO_3^-$, or $C_8H_{17}PhSO_3^-$) hereafter denoted as MC_nX. The presence of thermotropic lamellar mesophases is evidenced in most of these materials, occurring in the Fe(II) materials at temperatures just above the spin crossover, which remains abrupt and complete.

EXPERIMENTAL SECTION

Methods. Infrared spectra were performed on KBr pellets with a FTIR 750 NICOLET (Magna-IR) spectrometer. Magnetization measurements at variable temperature have been performed using a Quantum Design MPMS-XL SQUID magnetometer, operating between 1.8 and 400 K, in applied dc magnetic fields ranging from −7 to 7 T. X-ray diffraction experiments at small angles (SAXS) were performed on a homemade experimental setup equipped with an oven working up to 150 °C.[19] Measurements at higher angles were performed on a Philips X'Pert powder diffractometer equipped with a high-temperature chamber. Differential scanning calorimetry (DSC) measurements were conducted on a Perkin-Elmer Pyris apparatus using closed aluminum pans. Thermal equilibration was verified at the starting and final temperatures of each scan using 1 min isotherms. Temperature and enthalpy calibrations were made with a standard sample of indium using its melting transition (156.6 °C, 3.296 kJ mol^{-1}). Excess enthalpies were deduced by subtracting a suitable baseline. Elemental analyses were done either on a Perkin-Elmer 2400 analyzer at Leiden University, The Netherlands, or by the CNRS Service Central d'Analyze, Solaize, France. Thermogravimetric experiments were performed with a Setaram TAG-1750. Measurements were done under air with ramps of 3 °C min^{-1}.

Materials. All solvents and reagents were obtained from commercial sources as analytical grade and used without further purification.

$Fe(ptol)_2$ and $Zn(ptol)_2$ hydrates were obtained by stirring, respectively, iron and zinc powder (0.5 mol per liter of solution) in a 100 mL aqueous solution of p-toluenesulfonic acid (1.5 mol/L) at 80 °C for 4 h. After filtration of the remaining metal solid, the filtrate was left cooling and standing at room temperature, allowing for crystallization by slow evaporation of water of, respectively, $Fe(ptol)_2{\cdot}6H_2O$ and $Zn(ptol)_2{\cdot}6H_2O$ crystals that were recovered by filtration and washed with cold water. The water content of the hydrates was determined by thermogravimetric analysis. $Zn(ptol)_2{\cdot}6H_2O$: yield 29.57 g (57%). Anal. Calcd (Found) for $ZnO_{12}C_{14}H_{26}S_2$: C, 32.60 (32.7); H, 5.08 (5.0); S, 12.43 (12.3). Selected IR data (KBr pellet, cm^{-1}): 3389 (br), 1642 (m), 1176 (s), 1122 (s), 1037 (s), 1010 (s), 810 (m), 677 (m). $Fe(ptol)_2{\cdot}6H_2O$: yield 27.40 g (54%). Anal. Calcd (Found) for $FeO_{12}C_{14}H_{26}S_2$: C, 33.21 (33.25); H, 5.18 (5.24); S, 12.67 (12.58). Selected IR data (KBr pellet, cm^{-1}): 3383 (br), 1644 (m), 1180 (s), 1122 (s), 1036 (s), 1009 (s), 812 (m), 675 (m).

$Fe(C_8H_{17}SO_3)_2$ and $Fe(C_8H_{17}PhSO_3)_2$ were obtained from $FeCl_2$ by substitution of the anion with $NaC_8H_{17}SO_3$ and $NaC_8H_{17}PhSO_3$, respectively. Both salts were stirred in water containing a small amount of ascorbic acid. The resulting suspension was filtered. The white compounds were isolated and dried over P_2O_5 under reduced pressure. Yields were between 60% and 70%. $Fe(C_8H_{17}SO_3)_2{\cdot}6H_2O$: Anal. Calcd (Found) for $FeO_{12}C_{16}H_{46}S_2$: C, 34.91 (34.95); H, 8.42 (8.50); S, 11.65 (11.61). Selected IR data (KBr pellet, cm^{-1}): 3369 (br), 2921 (m), 2849 (m), 1657 (m), 1470 (w), 1193 (s), 1139 (s), 1043 (s), 608 (s). $Fe(C_8H_{17}PhSO_3)_2{\cdot}6H_2O$: Anal. Calcd (Found) for $FeO_{12}C_{28}H_{54}S_2$: C, 47.86 (47.91); H, 7.75 (7.79); S, 9.13 (9.10). Selected IR data (KBr pellet, cm^{-1}): 3376 (br, w), 2917 (m), 2848 (m), 1623 (m), 1465 (s), 1219 (s), 1158 (s), 1133 (s), 1050 (s), 1014 (m), 696 (m), 608 (s).

4-*n*-Alkyl-1,2,4-triazole ligands were prepared as previously described.[20]

Coordination polymers of formula $[M(4\text{-}n\text{-alkyl-1,2,4-triazole})_3]A_2{\cdot}xH_2O$ were synthesized following the same procedure: a hot ethanolic solution (7 mmol, 40 mL) of the 4-*n*-alkyl-1,2,4-triazole was added slowly to an aqueous solution of the iron(II) or zinc(II) salt (2 mmol, 20 mL) containing in the iron(II) cases a small amount of ascorbic acid to prevent oxidation to iron(III). A white precipitate formed rapidly upon addition. After 30 min aging, the solution was filtered and the solid washed with successively 2 × 40 mL of water, 20 mL of a 50:50 V/V water/ethanol mixture, and 2 × 50 mL ethanol. After drying, the iron compounds turned purple, indicating the presence of iron(II) ions in a low-spin state. The yields were between 75% and 86%. The formula, and in particular the water content x (that was found to range from 1 to 4), of the coordination polymers were determined by elemental and thermogravimetric analysis. Satisfactory elemental analysis, IR bands, and thermogravimetric data were obtained for all compounds.

$[Zn(C_{10}H_{21}trz)_3](Cl)_2{\cdot}2H_2O$. Anal. Calcd (Found) for $ZnC_{36}H_{73}N_9O_2Cl_2$: C, 54.0 (54.4); H, 9.2 (9.2); N, 15.7 (15.9). Selected IR data (KBr pellet, cm^{-1}): 3404 (br), 3110 (m), 2954 (m), 2919 (s), 2851 (s), 1553 (m), 1468 8 m), 1397 (w), 1194 (m), 1078 (m), 1037 (m), 977 (w), 884 (br), 721 (m), 663 (w), 636 (m).

$[Zn(C_{11}H_{23}trz)_3](Cl)_2{\cdot}4H_2O$. Anal. Calcd (Found) for $ZnC_{39}H_{83}N_9O_4Cl_2$: C, 53.3 (53.5); H, 9.5 (8.9); N, 14.4 (14.4). Selected IR data (KBr pellet, cm^{-1}): 3410 (br), 3110 (m), 2953 (m), 2918 (s), 2851 (s), 1553 (m), 1467 (m), 1397 (w), 1194 (m), 1078 (m), 1037 (m), 977 (w), 885 (br), 722 (m), 663 (w), 637 (m).

dx.doi.org/10.1021/ic300404r | Inorg. Chem. 2012, 51, 5417−5426

[Zn(C$_{13}$H$_{27}$trz)$_3$](Cl)$_2$·4H$_2$O. Anal. Calcd (Found) for $ZnC_{45}H_{95}N_9O_4Cl_2$: C, 56.2 (56.3); H, 10.0 (9.5); N, 13.1 (13.2). Selected IR data (KBr pellet, cm^{-1}): 3430 (br), 3110 (m), 2954 (m), 2917 (s), 2850 (s), 1552 (m), 1468 (m), 1394 (w), 1193 (m), 1077 (m), 1035 (m), 976 (w), 887 (br), 722 (m), 664 (w), 650 (m), 637 (m).

[Zn(C$_{16}$H$_{33}$trz)$_3$](Cl)$_2$·2H$_2$O. Anal. Calcd (Found) for $ZnC_{54}H_{109}N_9O_2Cl_2$: C, 61.6 (61.8); H, 10.4 (10.2); N, 12.0 (12.1). Selected IR data (KBr pellet, cm^{-1}): 3440 (br), 3110 (m), 2953 (m), 2918 (s), 2850 (s), 1553 (m), 1469 (m), 1397 (w), 1194 (m), 1078 (m), 1037 (m), 978 (w), 887 (br), 720 (w), 663 (w), 638 (m).

[Zn(C$_{18}$H$_{37}$trz)$_3$](Cl)$_2$·2H$_2$O. Anal. Calcd (Found) for $ZnC_{60}H_{121}N_9O_2Cl_2$: C, 63.4 (63.7); H, 10.7 (10.6); N, 11.1 (11.2). Selected IR data (KBr pellet, cm^{-1}): 3437 (br), 3110 (m), 2954 (m), 2918 (s), 2850 (s), 1553 (m), 1469 (m), 1397 (w), 1194 (m), 1079 (m), 1037 (m), 978 (w), 887 (br), 721 (m), 663 (w), 639 (m).

[Zn(C$_{18}$H$_{37}$trz)$_3$](ptol)$_2$·2H$_2$O. Anal. Calcd (Found) for $ZnC_{74}H_{135}N_9O_8S_2$: C, 63.1 (63.5); H, 9.7 (9.6); N, 8.9 (9.0); S, 4.5 (4.3). Selected IR data (KBr pellet, cm^{-1}): 3095 (br), 3023 (w), 2955 (m), 2920 (s), 2850 (s), 1568 (m), 1458 (m), 1402 (w), 1214 (s), 1196 (s), 1124 (s), 1036 (s), 1012, (s) 815 (m), 721 (w), 682 (m), 646 (w), 568 (m).

[Fe(C$_{10}$H$_{21}$trz)$_3$](Cl)$_2$·3H$_2$O. Anal. Calcd (Found) for $FeC_{36}H_{75}N_9O_3Cl_2$: C, 53.5 (53.3); H, 9.4 (9.4); N, 15.6 (16.0). Selected IR data (KBr pellet, cm^{-1}): 3370 (br), 3058 (w), 2957 (m), 2925 (s), 2855 (s), 1555 (m), 1465 (m), 1415 (w), 1209 (m), 722 (w), 640 (m).

[Fe(C$_{13}$H$_{27}$trz)$_3$](Cl)$_2$·3H$_2$O. Anal. Calcd (Found) for $FeC_{45}H_{93}N_9O_3Cl_2$: C, 57.8 (58.1); H, 10.0 (10.0); N, 13.5 (13.4). Selected IR data (KBr pellet, cm^{-1}): 3380 (br), 3054 (w), 2957 (m), 2922 (s), 2853 (s), 1554 (m), 1466 (m), 1415 (w), 1210 (m), 722 (w), 641 (w).

[Fe(C$_{16}$H$_{33}$trz)$_3$](Cl)$_2$·4H$_2$O. Anal. Calcd (Found) for $FeC_{54}H_{111}N_9O_4Cl_2$: C, 60.1 (59.3); H, 10.5 (10.4); N, 11.7 (11.4). Selected IR data (KBr pellet, cm^{-1}): 3390 (br), 3055 (w), 2956 (m), 2921 (s), 2852 (s), 1554 (m), 1468 (m), 1415 (w), 1207 (m), 721 (w), 642 (w).

[Fe(C$_{18}$H$_{37}$trz)$_3$](Cl)$_2$·H$_2$O. Anal. Calcd (Found) for $FeC_{60}H_{119}N_9OCl_2$: C, 65.0 (65.4); H, 10.8 (11.1); N, 11.4 (11.4). Selected IR data (KBr pellet, cm^{-1}): 3391 (br), 3053 (w), 2956 (m), 2919 (s), 2850 (s), 1553 (m), 1468 (m), 1414 (w), 1211 (m), 721 (w), 642 (w).

[Fe(C$_{10}$H$_{21}$trz)$_3$](ptol)$_2$·2H$_2$O. Anal. Calcd (Found) for $FeC_{50}H_{87}N_9O_8S_2$: C, 56.5 (56.6); H, 8.3 (8.2); N, 11.9 (12.1) ; S 6.0 (5.7). Selected IR data (KBr pellet, cm^{-1}): 3480 (br), 3088 (m), 3018 (w), 3055 (m), 2925 (s), 2854 (s), 1558 (m), 1467 (m), 1401 (w), 1215 (s), 1193 (s), 1124 (s), 1035 (s), 1012 (s), 814 (m), 720 (w), 683 (s), 646 (w), 568 (m).

[Fe(C$_{13}$H$_{27}$trz)$_3$](ptol)$_2$·2H$_2$O. Anal. Calcd (Found) for $FeC_{59}H_{105}N_9O_8S_2$: C, 59.6 (60.1); H, 8.9 (9.3); N, 10.6 (10.6); S, 5.4 (5.0). Selected IR data (KBr pellet, cm^{-1}): 3487 (br), 3090 (m), 3018 (w), 2956 (m), 2927 (s), 2855 (s), 1556 (m), 1466 (m), 1401 (w), 1215 (s), 1194 (s), 1126 (s), 1036 (s), 1012 (s), 815 (m), 721 (w), 685 (s), 646 (w), 569 (m).

[Fe(C$_{16}$H$_{33}$trz)$_3$](ptol)$_2$·H$_2$O. Anal. Calcd (Found) for $FeC_{68}H_{121}N_9O_7S_2$: C, 63.0 (63.3); H, 9.4 (9.9); N, 9.7 (9.5); S, 5.0 (4.7). Selected IR data (KBr pellet, cm^{-1}): 3510 (br), 3087 (m), 3020 (w), 2956 (m), 2923 (s), 2853 (s), 1560 (m), 1469 (m), 1400 (w), 1217 (s), 1190 (s), 1124 (s), 1035 (s), 1013 (s), 815 (m), 722 (w), 683 (s), 646 (w), 565 (m).

Fe(C$_{18}$H$_{37}$trz)$_3$](ptol)$_2$·2H$_2$O. Anal. Calcd (Found) for $FeC_{74}H_{135}N_9O_8S_2$: C, 63.5 (63.3); H, 9.7 (9.8); N, 9.0 (9.0); S, 4.6 (4.7). Selected IR data (KBr pellet, cm^{-1}): 3490 (br), 3086 (m), 3018 (w), 2959 (m), 2925 (s), 2855 (s), 1560 (m), 1470 (m), 1400 (w), 1215 (s), 1193 (s), 1125 (s), 1038 (s), 1011 (s), 814 (m), 721 (w), 683 (s), 646 (w), 569 (m).

[Fe(C$_{18}$H$_{37}$trz)$_3$](C$_8$H$_{17}$SO$_3$)$_2$·H$_2$O. Anal. Calcd (Found) for $FeC_{76}H_{153}N_9O_7S_2$: C, 64.1 (64.0); H, 10.8 (10.9); N, 8.8 (8.9); S, 4.5 (4.6). Selected IR data (KBr pellet, cm^{-1}): 3344 (br), 2918 (s), 2846 (m), 1658 (m), 1468 (w), 1379 (w), 1212 (s), 1175 (s), 1141 (s), 712 (w), 603 (w).

[Fe(C$_{18}$H$_{37}$trz)$_3$](C$_8$H$_{17}$PhSO$_3$)$_2$·H$_2$O. Anal. Calcd (Found) for $FeC_{88}H_{161}N_9O_7S_2$: C, 67.8 (67.8); H, 10.3 (10.4); N, 8.0 (8.2); S, 4.1 (4.0). Selected IR data (KBr pellet, cm^{-1}): 3444 (br), 3092 (m), 2921 (s), 2851 (s), 1681 (m), 1558 (m), 1380 (w), 1217 (s), 1195 (s), 1124 (w), 1035 (m), 1012 (m), 694 (w).

RESULTS AND DISCUSSION

Synthesis and Spectroscopic Observations. The chloride and organosulfonate anions were selected for this study. One-dimensional triazole Fe(II) coordination polymers with these anions are expected to display SC phenomenon around or above room temperature.[13,18] Bromide or iodide ions were discarded despite their potential high SC temperatures due to the observation of decomposition at low temperatures for some triazole derivatives.[21] Zn(II) analogues were also synthesized to allow comparison with a more stable and diamagnetic system. In addition to the different response of the diamagnetic or paramagnetic mesophase under an applied dc magnetic field, these Zn analogues allow one to study a structurally similar system without facing oxidation issues known in the Fe(II) compounds. Indeed, liquid-crystal phases have been described in the Fe(II)/triazole system, but no characteristic optical texture was reported in any of the few reports so far.[14,15] In thermotropic LC, characteristic textures are usually observed by polarized optical microscopy cooling the systems from their isotropic liquid to the LC phase. In the case of Fe(II) systems, this technique becomes problematic as it faces their partial oxidization/decomposition at temperatures required to achieve the isotropic phase.

Coordination polymers were synthesized as previously reported by reacting an aqueous solution of the Zn(II) or Fe(II) salt with an excess of the alkyl-triazole dissolved in hot ethanol. Upon addition of the ethanol solution of triazole, a white precipitate forms immediately for the longer alkyl substituents and within minutes for the decyl one. It is worth mentioning that it is important to keep the precipitate in contact with the solution for at least 20 min before recovering the solid material. Below this aging time, the SC phenomenon observed for the Fe(II) compounds is systematically more gradual and less complete. These "truncated" properties are due to the presence of shorter oligomers for which the terminal Fe(II) ions does not exhibit a SC as observed for the trinuclear Fe(II)/triazole systems.[22] As a consequence, the intrinsic cooperativeness arising from triple N1,N2-triazole bridges along the chain is thus significantly reduced.

The 1,2-coordination mode of the triazole rings is confirmed by IR spectroscopy (Figure S1, Supporting Information). In all cases including for the Zn(II) compounds, a shift of the aromatic $\tilde{\nu}_{C-H}$ vibrations and of the ring bands in the range 1300−1500 cm^{-1} (depending on the nature of the metal center and the counteranion) is systematically observed. Moreover, the intensities of the ring torsion vibration modes of the triazoles around 670 cm^{-1} are very weak as expected when the local triazole ring symmetry is C_{2v}.[23] UV−vis absorption spectra for the Fe(II) compounds with Cl$^-$ and ptol$^-$ anions at room temperature are dominated by the $^1A_1$ to $^1T_1$ band around 550 nm, thus confirming the LS state of the materials. The presence of a very weak and broad band around 800 nm is revealing traces of HS Fe(II) ions ascribed to the Fe(II) ions located at the polymeric chain ends. In air, the iron compounds were found to decompose just before or during the melting in the 170−210 °C temperature range, turning to a typical brown color. This was not the case for the zinc compounds in agreement with an oxidation process of the iron ones.

Magnetic and Thermal Signatures of the Spin Crossover. The thermal spin crossover of most of the Fe(II) compounds reported here has been previously described.[18a,b,20]

dx.doi.org/10.1021/ic300404r | Inorg. Chem. 2012, 51, 5417−5426

The reproducibility of their properties was checked, and the typical thermal variation of the χT product (where χ is the molar magnetic susceptibility) is given in Figure 1 and Figures S2

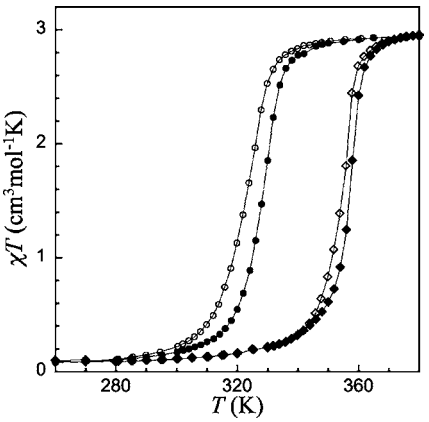

Figure 1. Temperature dependence of the product χT on cooling (empty symbols) and heating (full symbols) modes for FeC_{18}ptol (circles) and FeC_{18}Cl (rhombs) at about 1 K/min under 1000 Oe.

and S3, Supporting Information, for $[Fe(C_{18}H_{37}trz)_3](X)_2$ ($X = Cl^-$, ptol$^-$, $C_8H_{17}PhSO_3^-$, and $C_8H_{17}SO_3^-$; the respective compounds are noted thereafter FeC_{18}Cl, FeC_{18}ptol, $FeC_{18}(C_8H_{17}PhSO_3)$, and $FeC_{18}(C_8H_{17}SO_3)$). Table 1 gathers SC parameters for all studied compounds. In the case of Cl^- and ptol$^-$ compounds, the SC occurs above room temperature and is abrupt, as evidenced by the sharp decrease of χT upon lowering the temperature from about 3.0 (value typical for an $S = 2$ HS configuration) to roughly 0.1 cm^3 K mol^{-1}. These spin crossover phenomena are reversible and present a small thermal hysteresis at a temperature sweeping rate of around 1 K/min. For complexes $FeC_{18}(C_8H_{17}PhSO_3)$ and $FeC_{18}(C_8H_{17}SO_3)$ containing long alkyl chain counterions, the χT values decrease very gradually when lowering the temperature, achieving 0.18 and 1.2 cm^3 K mol^{-1} at 60 K for $FeC_{18}(C_8H_{17}PhSO_3)$ and $FeC_{18}(C_8H_{17}SO_3)$ respectively.

Although the χT product at low temperatures does reach very small values, it is not zero, as would be expected for a pure diamagnetic state. This residual paramagnetism is due to the Fe(II) ions situated at the coordination polymer chain ends that possess a HS ground state as also detected by absorption spectroscopy (vide supra). As observed for trinuclear complexes,[22] the HS Fe(II) sites are stabilized by different coordination spheres, including either water or monocoordinated triazole ligands. Thus, the amount of residual paramagnetism is an indirect probe of the average length of the polymeric chains. The very high residual paramagnetism observed in previous studies[14,15] therefore corresponds to small oligomeric chains, as indeed expected with the counteranions like ClO_4^- or long substituents on the triazole ring.[20] On the other hand, the results obtained here with Cl^- and ptol$^-$ anions indicate and confirm the almost complete SC and thus long polymeric Fe(II) chains.

The spin crossover of these materials is also detected by DSC technique (see below and Table 1), with a broad peak centered at temperatures that are in good agreement with the magnetic properties. The associated enthalpies are relatively high, ranging from 3.0 to above 20.0 kJ/mol, as usually observed in the presence of a marked cooperative character of the spin crossover. Therefore, these values are expected for these polymeric materials as recently studied in detail.[24]

Solid-State Structure. Selected powder diffraction patterns of the reported materials are shown in Figure 2. As previously observed, the 1D triazole-based Fe(II) materials are poorly crystalline. Indeed, the one-dimensional linear structure of this type of materials, shown in Scheme 1, was initially demonstrated by EXAFS, XANES, and WAXS studies[25] by comparison with trinuclear complexes for which the crystallographic structure is known.[22] Only very recently in 2011 the structure of $[Fe(Htrz)_2(trz)](BF_4)$ and $[Fe(NH_2trz)_3](NO_3)_2 \cdot nH_2O$ could be determined respectively by modulation enhanced X-ray powder diffraction[26] and single-crystal X-ray diffraction.[8] On the other hand, the Zn(II) compounds present well-defined powder X-ray patterns (see Figure 2). This is also the case of Cu(II) derivatives for which the structure could be solved from single-crystal diffraction.[27] Overall, all previous

Table 1. Parameters Describing the Structural Arrangement and the SC Properties of MC_nX Compounds

compound	d_{RT}/d_{LC} (Å)	$T_{SC}/\Delta T$ (K, from χT vs T)[a]	T_{SC} (K, from DSC)[b]	T_m (K)[c]	ΔH_m (kJ mol^{-1})	T_{clear} (K)[c]	ΔH_{clear} (kJ mol^{-1})
ZnC_{18}Cl	26.8/32.5	N/A	N/A	409	78.6	485	4.3
ZnC_{16}Cl	23.7/29.6	N/A	N/A	410	65.5	481	4.1
ZnC_{13}Cl	20.1/25.8	N/A	N/A	417	71.3	462	4.8
ZnC_{11}Cl	−/23.0	N/A	N/A	431	68.7	[427]	2.9
ZnC_{10}Cl		N/A	N/A	424	61.6	[384]	1.4
ZnC_{18}ptol		N/A	N/A	430	15	506	35
FeC_{18}Cl	48/33	357/3	363	419	11.9	476	1.3
FeC_{16}Cl		358/6	362	421	7.0	477	1.0
FeC_{13}Cl			364	426	2.5	480	1.8
FeC_{10}Cl		338/4	362	422	4.7	460	1.0
FeC_{18}ptol	38.2/26.6	328/6	310	451	19.3	543	1.7
FeC_{16}ptol	33.2/25.1	328/5	327	455	19.4	543	1.5
FeC_{13}ptol	30.3/23.4	295/10	330	455	14.1	546	2.4
FeC_{10}ptol		335/2	326	469	4.4		
$FeC_{18}(C_8H_{17}PhSO_3)$		244	242				
$FeC_{18}(C_8H_{17}SO_3)$		278	294	450	3.0		

[a] T_{SC} are those upon warming, ΔT being the hysteresis width at a 1 K/min sweeping rate. [b] Temperature of the peak maximum upon warming, since in some cases determination of a correct baseline is difficult, making the onset of the peak poorly defined. [c] T_m and T_{clear} are derived from the DSC peak maxima; values in brackets indicate the clearing temperature from the monotropic phase.

dx.doi.org/10.1021/ic300404r | Inorg. Chem. 2012, 51, 5417−5426

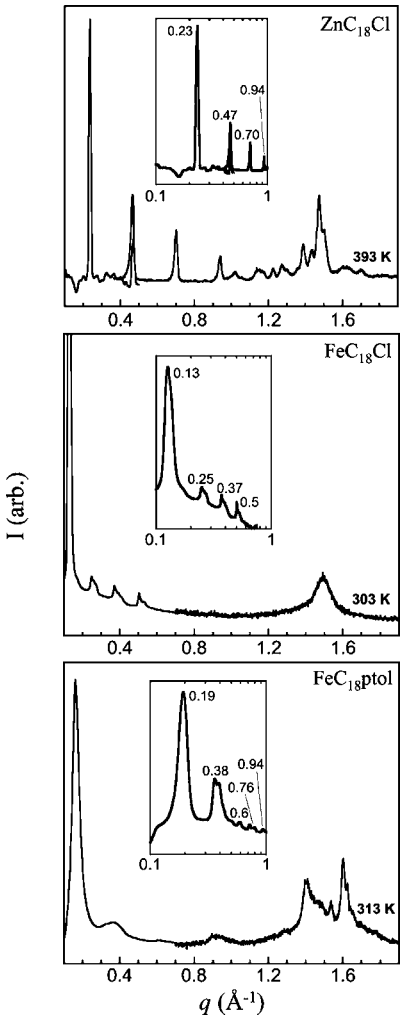

Figure 2. X-ray powder diffraction patterns in the (crystalline) solid state for $ZnC_{18}Cl$ (top), $FeC_{18}Cl$ (middle), and $FeC_{18}ptol$ (bottom). Exact temperatures are indicated in each graph. Insets show the log–log plot of the low angle area. Data are taken from two separate measurements on two experimental set ups for small-angle and wide-angle ranges (see Experimental Section).

Scheme 1. Representation of (a) 4-*n*-Alkyl-1,2,4-triazole ligands, (b) the 1D Chain Formed through Triple N1–N2 Bridges upon Coordination to Fe(II) or Zn(II) Ions (shown as orange balls, nitrogen and carbon are, respectively, depicted as blue and gray), and (c) the Space Fill Idealized Conformation of One of These Bridges with Fully-Stretched Decyl Substituent on the Triazole Ring

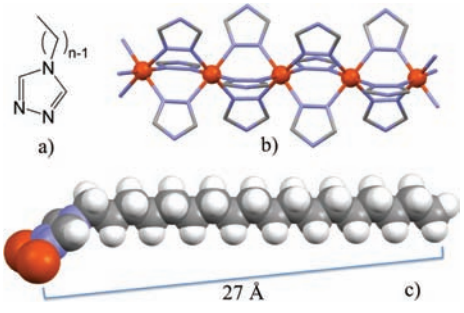

structural information available on these triazole-based materials agree with the presence of M(II) chains linked by triple N1,N2 triazole bridges that are disposed in an eclipsed alternating propeller disposition along the polymeric chains.

The alkyl substituents in the present systems are thus approximately pointing perpendicular to the chain direction in (at least) six directions. In agreement with this schematic view (see Scheme 1), the room temperature small angle XRD diffractograms of all Zn(II) and Fe(II) compounds studied here are dominated by an intense peak at low q. Diffraction peaks with q ratios of 1:2:3:4 are observed as the signature of a lamellar organization. This strong diffraction can clearly be ascribed to interchain metal–metal separation as the position of the main peak is influenced by the length of the alkyl chains. The diffraction at higher q, corresponding to organization at shorter distances and thus within the coordination chains, is very poor for the Fe compounds, although a more intense peak or massif is detected in all Zn and Fe compounds in the range 1.4–1.6 $Å^{-1}$. Overall, the MC_nX compounds studied here can be pictured as packed rod-like polymers separated by alkyl arms and organized in layers, as indirectly confirmed by the observation of textures in optical microscopy typical of a liquid-crystalline lamellar phase (vide infra).

The interlamellar distances d, gathered in Table 1, are derived from the position of the main peaks using $d = 2\pi/q$. Assuming fully stretched alkyl chains, the diameter of the cylinder formed by one coordination Fe(II)/triazole chain could reach at most 32 Å for n = 10 to 47 Å for n = 18. The determined interlamellar distances for the ZnC_nCl compounds (Table 1), in other words the interchain metal–metal distances, are all much smaller, indicating that the alkyl chains are interdigitated and/or folded. The variation of the interlamellar distance d with the length of the alkyl chain n is shown in Figure 3 for the ZnC_nCl system. d is a linear function of n,

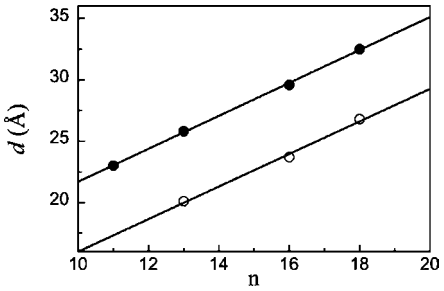

Figure 3. Interlamellar distance d as a function of n, the length of the 4-*n*-alkyl substituent on the triazole ligand, for the series ZnC_nCl in the solid crystalline state (empty circles) and in the mesophase at 430–440 K (full circles).

suggesting a similar structural organization in all compounds of the series. The slope of the linear regression is 1.33 Å. This value is slightly higher than one C–C bond (ca. 1.25 Å in trans conformation), confirming the strong interdigitation of the alkyl arms, which is certainly reinforcing the good cohesion between the coordination M(II)/triazole chains (note that in the absence of interdigitation, the slope should be equal to two C–C bonds). On the other hand, the interlamellar distance in $FeC_{18}Cl$ amounts to 48 Å, indicating the absence or at best the weak alkyl chain interdigitation in this material. The data for the FeC_nptol series in the solid state show a less pronounced decrease of d with decreasing n and no clear linear trend (Figure S4, Supporting Information). These observations agree with the much poorer crystallinity of the Fe-containing solids

dx.doi.org/10.1021/ic300404r | Inorg. Chem. 2012, 51, 5417–5426

(Figure 2) and likely indicate amorphous folding of the alkyl chains in the latter case.

Mesomorphic Behavior. Such rod-shaped molecules with peripheral divergent alkyl chains may self-organize as columnar or lamellar phases as observed in polycatenars or neat soaps.[28] Indeed, most compounds studied here possess thermotropic liquid crystal properties. The mesophases have been studied by polarized optical microscopy (POM), differential scanning calorimetry (DSC), and X-ray scattering. The structural, thermal, and thermodynamic data are collected in Table 1. It is well known that the liquid-crystal phases are very dependent on the purity of the mesogenic molecules or complexes; therefore, the tendency of the Fe compounds to partially oxidize at temperatures as low as 180 °C (453 K) makes their study more complicated. For this reason, we first investigated in great detail the more stable zinc analogues.

Zn(II)/Triazole Systems. Polarized optical microscopy of $ZnC_{18}Cl$ reveals a phase transition from a crystalline phase to a birefringent one at ca. 409 K with a clearing point to the isotropic liquid state at ca. 485 K. The observed focal conic textures are typical for a lamellar phase, as shown in Figure 4a. These

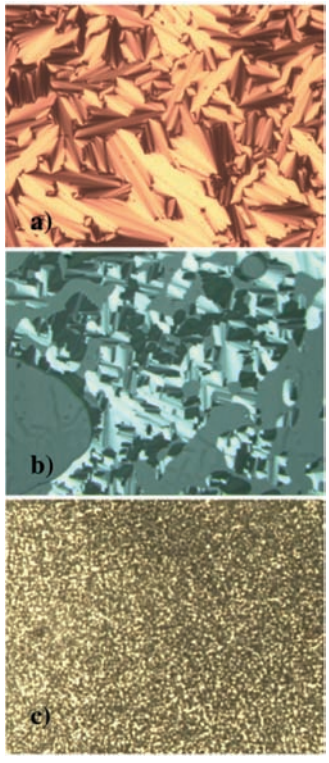

Figure 4. Polarized optical microscopic textures observed for $ZnC_{18}Cl$ (a) and $ZnC_{13}Cl$ (b) at 481 and 440 K, respectively, upon cooling from the isotropic liquid and $FeC_{18}ptol$ (c) at 480 K upon warming from room temperature.

observations are perfectly reversible, and textures are indeed better observed after cooling from the isotropic liquid (I).

The compounds with a smaller alkyl substituent on the triazole ring show a similar behavior down to C_{13}, only differing in the Cr → lamellar transition and the clearing temperatures (Table 1). For $ZnC_{10}Cl$ and $ZnC_{11}Cl$, textures corresponding to the lamellar mesophase could only be observed upon cooling from the isotropic liquid, thus indicating a monotropic phase, which was confirmed by DSC experiments (vide infra). These compounds present a tendency toward homeotropic anchoring. Indeed, between simple glass slides and under a crossed polarizer and analyzer some birefringence is observed fugaciously (Figure S5, Supporting Information) and rapidly disappears, leaving a black texture, thus indicating the perpendicular orientation of molecules with respect to the substrate. Special glass cells treated to favor a flat organization have thus been used, allowing observation of stable focal conic textures over large areas. For the shorter alkyl chain compounds, even under these conditions, the homeotropic tendency subsists and textures can only be observed in small domains, as shown in Figure 4b for $ZnC_{13}Cl$.

X-ray diffraction measurements (Figure 5) in the adequate temperature range confirm the appearance of a lamellar phase.

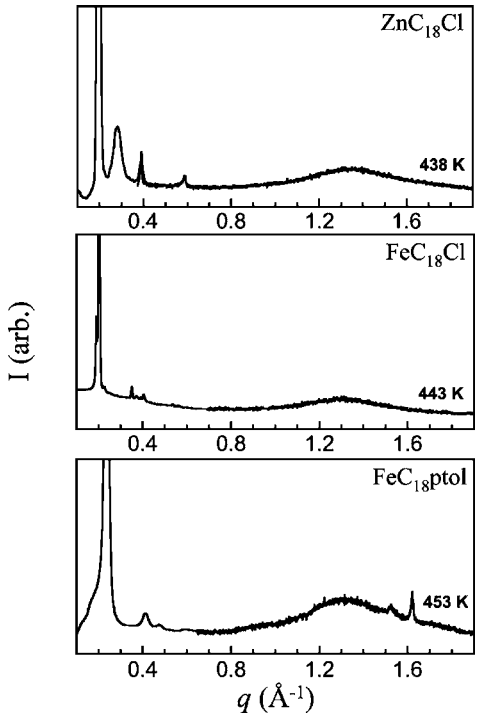

Figure 5. X-ray powder diffraction patterns in the mesophase for $ZnC_{18}Cl$ (top), $FeC_{18}Cl$ (middle), and $FeC_{18}ptol$ (bottom). Exact temperatures are indicated in each graph. Data are taken from two separate measurements on two experimental set ups for small-angle and wide-angle ranges (see Experimental Section).

For $ZnC_{18}Cl$, the wide-angle diffraction in this temperature range shows only a very broad peak at q = 1.3 Å that can be ascribed to the average separation between alkyl chains within a partially organized fluid mesophase.

At small angles, intense peaks with a q ratio of 1:2:3 are still observed, in agreement with a lamellar mesophase, as revealed by POM. All thermally induced modifications are perfectly reversible in all the Zn-containing compounds studied. As expected, the interlamellar distance is systematically higher in the mesophase than in the crystal state, although a linear dependence (Figure 3) on the alkyl chain length n remains with almost the same slope (1.34 Å). Hence, the alkyl arms remain interdigitated even in the liquid crystal phase. Extrapolation to n = 0 gives a value of 8.5 Å, which is in reasonable agreement with the diameter of a cylinder made of a $[Zn(trz)_3]_n$ core, estimated at 7 Å. The schematized structural organization of the mesophase in layers of coordination polymers is depicted in Scheme 2.

Differential scanning calorimetry (DSC) data for $ZnC_{18}Cl$ and $ZnC_{10}Cl$ are shown in Figure 6 as representative for the

dx.doi.org/10.1021/ic300404r | Inorg. Chem. 2012, 51, 5417−5426

Scheme 2. Schematic Representation of (a) a Hexacatenar Moiety That Would Form Repetitive Triple 4-Octadecyl-1,2,4-triazole Bridges with Fully-Stretched Alkyl Arms in Eclipsed Conformation and (b and c) Lamellar Packing of the Resulting Rods with Interdigitation, Respectively, Perpendicular and Parallel to the Average Rod Axis

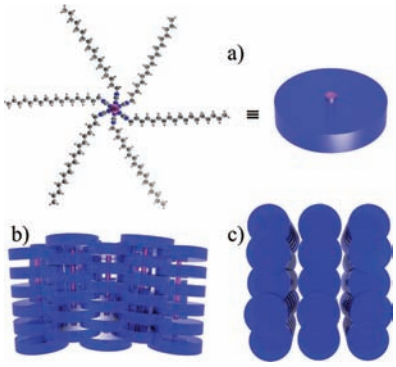

rest of the compounds (whose data are given in the Supporting Information, Figure S6). These measurements are in good agreement with POM observations and the existence of mesophases. Indeed, DSC traces of ZnC_nCl (n = 18, 16, 13) reproducibly show two endothermic peaks upon warming, clearly associated by pairs with two exothermic ones upon cooling. These two characteristic anomalies occur at temperatures similar to those observed by POM, corresponding to the Cr → lamellar phase transition and the clearing point. Systematically, the lower temperature peaks have a much higher associated enthalpy (65−79 kJ mol^{-1}) than the peaks at higher temperatures (between 4.1 and 4.8 kJ mol^{-1}). This observation confirms the POM conclusions that ascribed the first peak to the melting of the crystalline solid to a liquid-crystalline phase existing over a large range of temperature up to the second peak corresponding to the clearing point and transition to the isotropic liquid. For $ZnC_{10}Cl$ and $ZnC_{11}Cl$, DSC traces exhibit only one melting peak from the crystalline phase to the isotropic liquid upon warming at, respectively, 424 and 431 K, indicating the mesophase does not form from the crystalline state. Upon cooling, a first poorly energetic peak (1.4 and 2.9 kJ mol^{-1}) appears, corresponding to the I → lamellar phase transition followed by a second peak with much larger associated enthalpies (61 and 69 kJ mol^{-1}) corresponding to crystallization from the lamellar phase at 353 and 350 K, respectively. When warming again from the lamellar phase, only a poorly energetic peak attributed to the transition toward the isotropic liquid is detected at 384 and 427 K, respectively (see inset in Figures 6 and S6, Supporting Information). In the case of $ZnC_{11}Cl$, this clearing point almost coincides with the normal melting temperature. These observations are typical of a monotropic liquid crystal phase, observed here in the cooling mode.

Gathering the data from POM, DSC, and PXRD measurements for the ZnC_nX compounds, the transition temperatures as a function of n, the alkyl chain length, have been plotted in a phase diagram shown in Figure 7. The clearing temperature in the series ZnC_nCl regularly increases with increasing n, from 384 K for n = 10 to 485 K for n = 18. On the other hand, the melting temperature decreases with increasing n, from 431 K for n = 10 to 409 K for n = 18. Thus, for n < 12, a monotropic mesophase is observed with $T_m > T_{clear}$, while for n > 12, the lamellar mesophase exists over a wide temperature range, reaching 76 K for n = 18. From the trend observed for

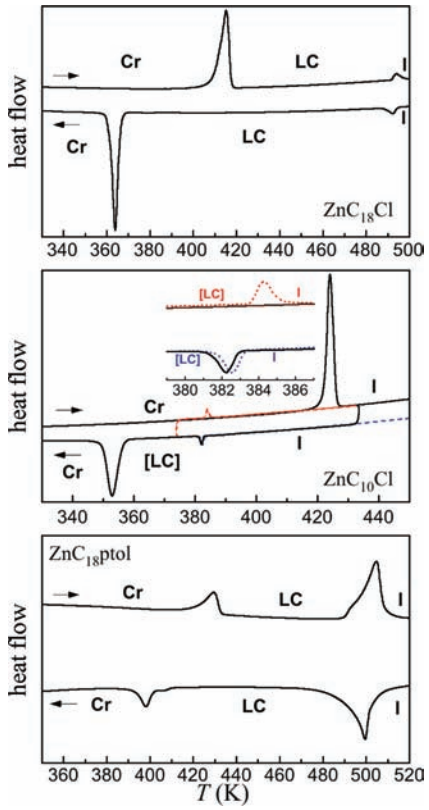

Figure 6. DSC traces of $ZnC_{18}Cl$ (top), $ZnC_{10}Cl$ (middle), and ZnC_{18}ptol (bottom) at 10 K/min, exhibiting heat flow humps associated with the transitions among the solid state (Cr), lamellar mesophase (LC), and isotropic liquid state (I). Arrows indicate the warming or cooling modes; endotherms are up. Inset of the figure middle shows experimental evidence of the monotropic mesophase [LC], occurring only in the cooling mode in the case of $ZnC_{10}Cl$ (see text).

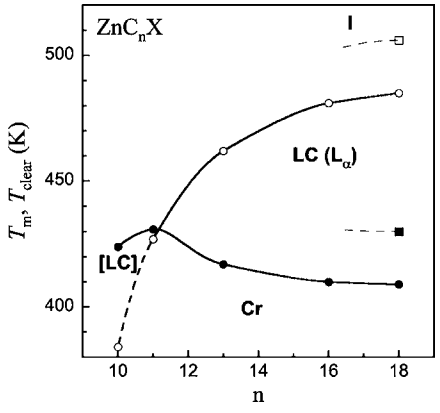

Figure 7. Phase diagram showing the temperature domains for the solid state (Cr), lamellar mesophase (LC, L_α is used to indicate a lamellar arrangement), and isotropic liquid state (I) for ZnC_nX and X = Cl (circles) and ptol (squares). Melting and clearing temperatures are represented by full and empty symbols, respectively. Lines are only guides for the eye.

n = 10−18 it is unlikely that longer alkyl substituents would result in a much larger clearing temperature or more importantly a lower melting temperature that would be necessary to observe the SC phenomenon within the mesophase. These transition temperatures are even found to be about 20 K higher in ZnC_{18}ptol,

dx.doi.org/10.1021/ic300404r | Inorg. Chem. 2012, 51, 5417−5426

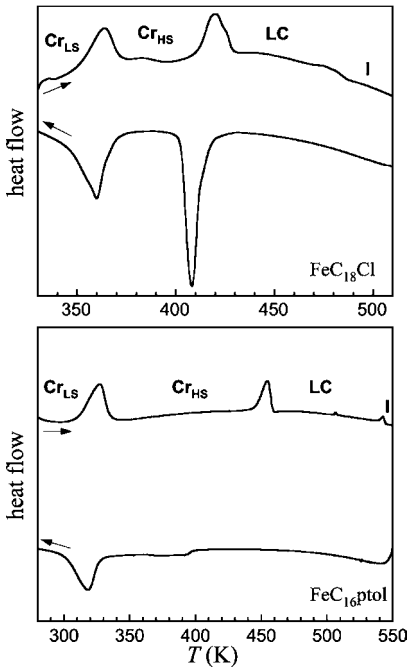

Figure 8. DSC traces of $FeC_{18}Cl$ (top) and $FeC_{16}ptol$ (bottom) at 10 K/min, exhibiting heat flow humps associated with the SC phenomenon and transitions among the solid state (Cr), lamellar mesophase (LC), and isotropic liquid state (I). Arrows indicate the warming or cooling mode; endotherms are up.

which is the reason why the full series was not studied with the $ptol^-$ anion.

Fe(II)/Triazole Systems. Besides the peak associated with the SC phenomenon in the 360−365 K range, the DSC traces of the FeC_nCl compounds upon warming (Figures 8 and S7, Supporting Information) are similar to those observed for the Zn compounds with a strong peak around 420 K followed by a much weaker peak in the 460−480 K range. By analogy to the Zn systems (vide supra), these peaks can be associated with a crystal to liquid crystal transition and the transition to isotropic phase, although the energies associated are about 4 times smaller with respect to the Zn analogues. Unfortunately, the compounds show signs of decomposition/oxidation, even at temperatures close to the melting and up to the clearing point. The FeC_nptol compounds (Figures 8 and S8, Supporting Information) exhibit a very similar behavior upon warming, with DSC traces showing peaks associated with the SC in the 310−330 K range, the melting to an intermediate lamellar phase in the 450−470 K range and a transition to an isotropic phase coupled to an evident partial decomposition around 545 K. For both Cl^- and $ptol^-$ compounds, the SC peak is observed upon cooling in a reproducible manner over several cycles, indicating the decomposition is only very partial since a large part of the material maintains its original magnetic properties. For all the Fe compounds, the poorly energetic peak (expected for the transition from the isotropic liquid to the mesophase) is absent of the DSC trace upon cooling from the isotropic liquid. Only a strong exothermic peak or a smooth step is observed for the Cl^- and $ptol^-$ compounds, probably due to crystallization/solidification. In the case of the $FeC_{18}(C_8H_{17}PhSO_3)$ and $FeC_{18}(C_8H_{17}SO_3)$ compounds with long alkyl chain counteranion, DSC traces show a broad peak at 242 and 294 K that corresponds to $Cr_{HS} \rightarrow Cr_{LS}$ spin crossover and a sharp peak at 364 and 341 K, respectively, on heating

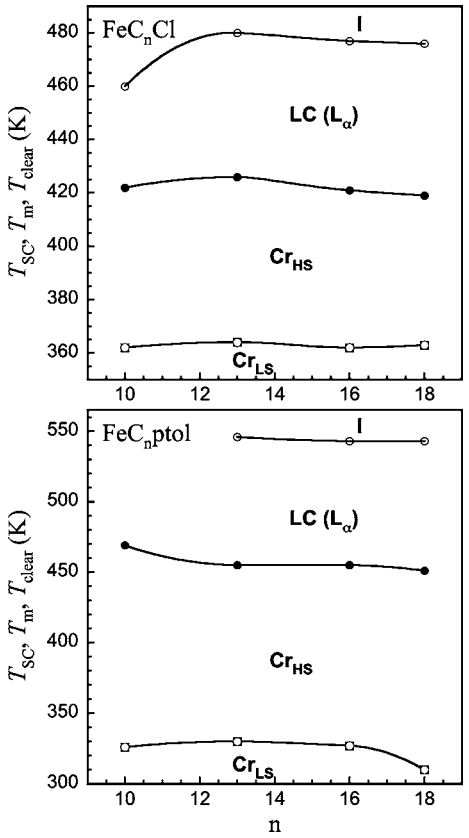

Figure 9. Phase diagrams showing the temperature domains for the solid state (Cr_{LS} and Cr_{HS}), pseudolamellar mesophase (LC, L_α is used to indicate a lamellar arrangement), and isotropic liquid state (I) for FeC_nCl (top) and FeC_nptol (bottom). SC, melting, and clearing temperatures are represented by square, full, and empty symbols, respectively, and all taken from DSC data. Lines are only guides for the eye.

mode. As no melting was observed by POM measurements at 364 and 341 K, the endothermic peak can only be attributed to a $Cr_{HS} \rightarrow Cr'_{HS}$ structural transition. It is worth mentioning that these phase transitions are reversible on cooling (Figure S9, Supporting Information). At higher temperature, only $FeC_{18}(C_8H_{17}SO_3)$ exhibits an weak endothermic peak at 450 K, which could be attributed to a $Cr'_{HS} \rightarrow$ LC phase transition based on POM observations. Unfortunately for both compounds, no isotropic peak is observed up to 530 K and above this temperature the compound decomposes very fast.

The existence of a lamellar liquid-crystalline phase is further supported by POM observations of birefringence at 480 K for the $FeC_{18}(ptol)$ in its liquid crystal phase (Figure 4c), although no clear texture could be observed. For the other Fe compounds (except $FeC_{18}(C_8H_{17}PhSO_3)$), birefringence in POM was observed at best in a transitory manner upon heating. Due to the decomposition of the Fe(II) compounds at temperatures lower than the clearing point, the POM textures of these systems are unfortunately extremely difficult to observe.

Powder X-ray diffractograms performed in the temperature range of existence of the mesophase show in all cases only one very broad peak at high angles centered at ca. 1.3 Å. This diffraction peak that corresponds to the alkyl "halo" as for the Zn compounds and the disappearance of the (poor) diffractions at high angles indicates formation of liquid-crystalline phase. In the small angle region, mostly one strong peak is observed to be very similar to that observed for the Zn analogues and thus

dx.doi.org/10.1021/ic300404r | Inorg. Chem. 2012, 51, 5417−5426

shifted toward larger q with respect to the low-temperature phase (see Figures 2 and 5). The higher order peaks associated with the lamellar phase are not observed in any of the Fe(II) materials. These X-ray diffraction results together with the difficulty to observe stable textures seem to indicate that the Fe compounds likely only exhibit a short-range preorganization without developing a real lamellar phase. This absence of long-range lamellar phase is probably the result of the poor crystallinity of the solid phase that may arise from shorter one-dimensional coordination chains and/or a broader distribution of their lengths. The presence of impurities arising from the oxidation/decomposition of a fraction of the material may also contribute to the weak stability of the thermotropic mesophase in the Fe compounds. Unfortunately, the decomposition/oxidation observed from temperatures just above the melting ($ptol^-$ compounds) or close to the clearing temperature (Cl^- and $C_8H_{17}SO_3^-$ compounds) impedes a deeper study of these phases.

Like for the Zn compounds, the melting and clearing temperatures have been gathered to build a pseudophase diagram, also including the transition from the LS to the HS state (Figure 9). In contrast to the ZnC_nCl series, these transition temperatures stay roughly constant with n for both for FeC_nCl and FeC_nptol systems, although the observed temperatures for $n = 18$ and thus the corresponding domains of existence of the mesophase are close to those determined for the Zn analogue (see Table 1). The absence of a significant influence of the alkyl arms length on the melting and clearing temperatures is likely to be related to the structural organization of the coordination Fe(II) polymer. In line with the variation of the interlamellar distance along the FeC_nptol series (vide infra, Figure S4), these results suggest an amorphous folding and noninterdigitation of the alkyl chains in the Fe(II) materials.

CONCLUSIONS

Zn(II) one-dimensional coordination polymers formed through triple N1,N2-4-*n*-alkyl-1,2,4-triazole (with $n = 10-18$) bridges and obtained with chloride and sulfonate anions display a thermotropic lamellar liquid-crystalline phase stable over a wide temperature range, for example, 409 to 485 K for $[Zn(C_{18}H_{37}trz)_3](Cl)_2$. For the shorter alkyl substituent (decyl, undecyl), the mesophase is monotropic and occurs only in the cooling mode. The Fe(II) analogues, besides presenting a cooperative spin crossover and its associated magnetic and optical signatures, maintain a similar thermotropic behavior, although only reaching a preorganization, probably as a consequence of poor size homogeneity/crystallinity and/or impurity formed through partial oxidation/decomposition at high temperatures. The SC phenomenon in these materials occurs above room temperature but still below the liquid-crystal temperature domains in such a way that the two phenomena do not influence each other. The derived phase diagrams indicate that the use of longer alkyl substituents ($n > 18$) on the triazole ligands would probably not allow lowering sufficiently the temperature domain of the mesophase. On the other hand, as shown by the $FeC_{18}(C_8H_{17}PhSO_3)$ and $FeC_{18}(C_8H_{17}SO_3)$ compounds, functionalization of the counteranions by a long alkyl chain is also not a good strategy to improve the mesomorphic behavior. These conclusions highlight the necessity to adopt branched alkyl substituents on triazole ligands or anions to bring both phenomena to a common temperature range. On the other hand, the use of stable diamagnetic Zn(II) analogues has proven to be very useful to study the comparatively less stable and less crystalline Fe(II) analogues. This strategy is currently being employed with branched substituents on the triazole ligands.

ASSOCIATED CONTENT

Supporting Information

FT-IR spectra, additional magnetic properties, and DSC measurements. This material is available free of charge via the Internet at http://pubs.acs.org.

AUTHOR INFORMATION

Corresponding Author

*E-mail: roubeau@unizar.es; clerac@crpp-bordeaux.cnrs.fr.

Notes

The authors declare no competing financial interest.

ACKNOWLEDGMENTS

This work was supported by the Centre National de la Recherche Scientifique (CNRS), the University of Bordeaux, the Conseil Régional d'Aquitaine, GIS Advanced Materials in Aquitaine (COMET Project), the ANR (NT09_469563, AC-MAGnets project), the Erasmus Mundus External Cooperation Window of the European Community Mobility Programme for the Ph.D. fellowship of Dr. D. Siretanu, and the Spanish National Council of Sciences CSIC (PIE to O.R.).

REFERENCES

(1) (a) Coronado, E.; Galán-Mascarós, J. R.; Gómez-García, C. J.; Laukhin, V. *Nature* **2000**, *408*, 447−449. (b) Miller, J. S. *Angew. Chem., Int. Ed.* **2003**, *42*, 27−29.

(2) (a) Gütlich, P.; Goodwin, H. A., Eds. *Topics in Current Chemistry*; 2004; Vols. *233, 234, 235*. (b) Gütlich, P. *Struct. Bonding (Berlin)* **1981**, *44*, 83−195. (c) Gütlich, P.; Garcia, Y.; Goodwin, H. A. *Chem. Soc. Rev.* **2000**, *29*, 419−427. (d) Gütlich, P.; Hauser, A.; Spiering, H. *Angew. Chem., Int. Ed. Engl.* **1994**, *33*, 2024−2054.

(3) (a) Vreugdenhil, W.; van Diemen, J. H.; de Graff, R. A. G.; Haasnoot, J. G.; Reedijk, J.; van der Kraan, A. M.; Kahn, O.; Zarembowitch, J. *Polyhedron* **1990**, *9*, 2971−2979. (b) Kröber, J.; Audière, J.-P.; Claude, R.; Codjovi, E.; Kahn, O.; Haasnoot, J. G.; Grolière, F.; Jay, C.; Bousseksou, A.; Linarès, J.; Varret, F.; Gonthier-Vassal, A. *Chem. Mater.* **1994**, *6*, 1404−1412. (c) Létard, J.-F.; Guionneau, P.; Codjovi, E.; Lavastre, O.; Bravic, G.; Chasseau, D.; Kahn, O. *J. Am. Chem. Soc.* **1997**, *119*, 10861−10862. (d) Niel, V.; Martinez-Agudo, J. M.; Muñoz, M. C.; Gaspar, A. B.; Real, J. A. *Inorg. Chem.* **2001**, *40*, 3838−3839. (e) Weber, B.; Bauer, W.; Obel, J. *Angew. Chem., Int. Ed.* **2008**, *47*, 10098−10101. (f) Craig, G. A.; Costa, J. S.; Roubeau, O.; Teat, S. J.; Aromí, G. *Chem.—Eur. J.* **2011**, *17*, 3120−3127.

(4) Gaspar, A. B.; Ksenofontov, V.; Seredyuk, M.; Gütlich, P. *Coord. Chem. Rev.* **2005**, *249*, 2661−2676.

(5) (a) Donnio, B.; Bruce, D. W. *Struct. Bonding (Berlin)* **1999**, *95*, 193−247. (b) Binnemans, K.; Görller-Walrand, C. *Chem. Rev.* **2002**, *102*, 2303−2346. (c) Serrano, J. L.; Sierra, T. *Coord. Chem. Rev.* **2003**, *242*, 73−85. (d) Piguet, C.; Bünzli, J. C. G.; Donnio, B.; Guillon, D. *Chem. Commun.* **2006**, *36*, 3755−3768. (e) Donnio, D.; Guillon, D.; Deschenaux, R.; Bruce, D. W. *Compr. Coord. Chem. II* **2003**, *7*, 357−627. (f) Gaspar, A. B.; Seredyuk, M.; Gütlich, P. *Coord. Chem. Rev.* **2009**, *253*, 2399−2413.

(6) Galyametdinov, Y.; Ksenofontov, V.; Prosvirin, A.; Ovchinnikov, I.; Ivanova, G.; Gütlich, P.; Haase, W. *Angew. Chem., Int. Ed.* **2001**, *40*, 4269−4271.

(7) (a) Hayami, S.; Danjobara, K.; Inoue, K.; Ogawa, Y.; Matsumoto, N.; Maeda, Y. *Adv. Mater.* **2004**, *16*, 869−872. (b) Hayami, S.; Motokawa, N.; Shuto, A.; Masuhara, N.; Someya, T.; Ogawa, Y.; Inoue, K.; Maeda, Y. *Inorg. Chem.* **2007**, *46*, 1789−1794.

(8) The first single-crystal structure of an Fe(II) triazole-based chain compound was only recently reported, see: Grosjean, A.; Daro, N.;

Kauffmann, B.; Kaiba, A.; Létard, J. F.; Guionneau, G. *Chem. Commun.* **2011**, *47*, 12382−12384.
(9) (a) Coronado, E.; Galán-Mascarós, J. R.; Monrabal-Capilla, M.; García-Martínez, J.; Pardo-Ibáñez, P. *Adv. Mater.* **2007**, *19*, 1359−1361. (b) Forestier, T.; Mornet, S.; Daro, N.; Nishihara, T.; Mouri, S.-I.; Tanaka, K.; Fouché, O.; Freysz, E.; Létard, J.-F. *Chem. Commun.* **2008**, 4327−4329. (c) Forestier, T.; Kaiba, A.; Pechev, S.; Denux, D.; Guionneau, P.; Etrillard, C.; Daro, N.; Freysz, E.; Létard, J.-F. *Chem.—Eur. J.* **2009**, *15*, 6122−6130. (d) Tokarev, A.; Salmon, L.; Guari, Y.; Nicolazzi, W.; Molnar, G.; Bousseksou, A. *Chem. Commun.* **2010**, *46*, 8011−8013. (e) Tokarev, A.; Salmon, L.; Guari, Y.; Molnar, G.; Bousseksou, A. *New J. Chem.* **2011**, *35*, 2081−2088. (f) Etrillard, C.; Faramarzi, V.; Dayen, J. F.; Létard, J. F.; Doudin, B. *Chem. Commun.* **2011**, *47*, 9663−9665. (g) Prins, F.; Monrabal-Capilla, M.; Osorio, E. A.; Coronado, E.; van der Zant, H. S. J. *Adv. Mater.* **2011**, *23*, 1545−1549.
(10) (a) Roubeau, O.; Colin, A.; Schmitt, V.; Clérac, R. *Angew. Chem., Int. Ed.* **2004**, *43*, 3283−3286. (b) Fujigaya, T.; Jiang, D.-L.; Aida, T. *Chem. Asian J.* **2007**, *2*, 106−113. (c) Rubio, M.; López, D. *Eur. Polym. J.* **2009**, *45*, 3339−3346.
(11) (a) Roubeau, O.; Agricole, B.; Clérac, R.; Ravaine, S. *J. Phys. Chem. B* **2004**, *108*, 15110−15116. (b) Thibault, C.; Molnár, G.; Salmon, L.; Bousseksou, A.; Vieu, C. *Langmuir* **2009**, *26*, 1557−1560. (c) Faulmann, C.; Chahine, J.; Malfant, I.; de Caro, D.; Cormary, B.; Valade, L. *Dalton Trans.* **2011**, *40*, 2480−2485. (d) Chen, C.; Ma, J.-G.; Zhang, J.-J.; Shi, W.; Cheng, P.; Liao, D.-Z.; Yan, S.-P. *Chem. Commun.* **2010**, *46*, 5073−5075.
(12) (a) Kahn, O.; Jay Martinez, C. *Science* **1998**, *279*, 44−48. (b) Létard, J.-F.; Guionneau, P.; Goux-Capes, L. *Top. Curr. Chem.* **2004**, *235*, 221−249.
(13) (a) Kahn, O; Codjovi, E. *Philos. Trans. R. Soc. London A* **1996**, *354*, 359−379. (b) Aromí, G.; Barrios, L. A.; Roubeau, O.; Gamez, P. *Coord. Chem. Rev.* **2011**, *255*, 485−546.
(14) Fujigaya, T.; Jiang, D.-L.; Aida, T. *J. Am. Chem. Soc.* **2003**, *125*, 14690−14691.
(15) (a) Seredyuk, M.; Gaspar, A. B.; Ksenofontov, V.; Reiman, S.; Galyametdinov, Y.; Haase, W.; Rentschler, E.; Gütlich, P. *Chem. Mater.* **2006**, *18*, 2513−2519. (b) Seredyuk, M.; Gaspar, A. B.; Ksenofontov, V.; Galyametdinov, Y.; Verdaguer, M.; Villain, F.; Gütlich, P. *Inorg. Chem.* **2008**, *47*, 10232−10245.
(16) Lee, Y. H.; Komatsu, Y.; Yamamoto, Y.; Kato, K.; Shimizu, T.; Ohta, A.; Matsui, T.; Hayami, S. *Inorg. Chem. Commun.* **2011**, *14*, 1498−1500.
(17) (a) Roubeau, O.; Natividad, E.; Agricole, B.; Ravaine, S. *Langmuir* **2007**, *23*, 3110−3117. (b) Grondin, P.; Roubeau, O.; Castro, M.; Saadaoui, H.; Colin, A.; Clérac, R. *Langmuir* **2010**, *26*, 5184−5195.
(18) (a) Haasnoot, J. G. In *Magnetism: a supramolecular function*; Kahn, O., Ed.; NATO Advanced Study Institute Series; Kluwer Academic Publishers: Dordrecht, 1996; Vol. *C 484*, p 299. (b) Haasnoot, J. G. *Coord. Chem. Rev.* **2000**, *200*−*202*, 131−185. (c) Berezovskii, G. A.; Bessergenev, Y. G.; Lavrenova, L. G.; Ikorskii, V. N. *Russ. J. Phys. Chem.* **2002**, *76*, 1246−1250. (d) Codjovi, E.; Sommier, L.; Kahn, O.; Jay, C. *New J. Chem.* **1996**, *20*, 2075. (e) Garcia, Y.; van Konningsbruggen, P. J.; Lapouyade, R.; Fournès, L.; Rabardel, L.; Kahn, O.; Ksenovontov, V.; Levchenko, G.; Gütlich, P. *Chem. Mater.* **1998**, *10*, 2426−2433. (f) Toyazaki, S.; Nakanishi, M.; Komatsu, T.; Kojima, N.; Matsumura, D.; Yokoyama, T. *Synth. Met.* **2001**, *121*, 1794−1795.
(19) Nguyen, H. T.; Bouchta, A.; Navailles, L.; Barois, P.; Isaert, N.; Twieg, R. J.; Maaroufi, A.; Destrade, C. *J. Phys. II Fr.* **1992**, *2*, 1889−1906.
(20) Roubeau, O.; Alcazar Gomez, J. M.; Blaskus, E.; Kolnaar, J. J. A.; Haasnoot, J. G.; Reedijk, J. *New J. Chem.* **2001**, *25*, 144−150.
(21) Haasnoot, J. G. Private communication.
(22) (a) Garcia, Y.; van Koningsbruggen, P. J.; Bravic, G.; Guionneau, P.; Chasseau, D.; Cascarano, G. L.; Moscovici, J.; Lambert, K.; Michalowicz, A.; Kahn, O. *Inorg. Chem.* **1997**, *36*, 6357−6365. (b) Vos, G.; Le Fêbre, R. A.; de Graaf, R. A. G.; Haasnoot, J. G.; Reedijk, J. *J. Am. Chem. Soc.* **1983**, *105*, 1682−1683. (c) Kolnaar, J. J. A.; van Dijk, G.; Kooijman, H.; Spek, A. L.; Ksenofontov, V.; Gütlich, P.; Haasnoot, J. G.; Reedijk, J. *Inorg. Chem.* **1997**, *36*, 2433−2440.
(23) Haasnoot, J. G.; Groeneveld, W. L. *Z. Naturforsch.* **1977**, *32b*, 533.
(24) Roubeau, O.; Castro, M.; Burriel, R.; Haasnoot, J. G.; Reedijk, J. *J. Phys. Chem. B* **2011**, *115*, 3003−3012.
(25) (a) Michalowicz, A.; Moscovici, J.; Kahn, O. *J. Phys. IV Fr.* **1997**, C2−633. (b) Verelst, M.; Sommier, L.; Lecante, P.; Mosset, A.; Kahn, O. *Chem. Mater.* **1998**, *10*, 980−985.
(26) Urakawa, A.; van Beek, W.; Monrabal-Capilla, M.; Galán-Mascarós, J. R.; Palin, L.; Milanesio, M. *J. Phys. Chem. C* **2011**, *115*, 1323−1329.
(27) (a) Garcia, Y.; van Koningsbruggen, P. J.; Bravic, G.; Guionneau, P.; Chasseau, D.; Cascarano, G. L.; Moscovici, J.; Lambert, K.; Michalowicz, A.; Kahn, O. *Inorg. Chem.* **1997**, *36*, 6357−6365. (b) Drabent, K.; Ciunik, Z. *Chem. Commun.* **2001**, 1254−1255. (c) Garcia, Y.; van Koningsbruggen, P. J.; Bravic, G.; Chasseau, D.; Kahn, O. *Eur. J. Inorg. Chem.* **2003**, 356−362.
(28) (a) Nguyen, H. T.; Destrade, C.; Malthtète, J. In *Handbook of Liquid Crystals*; Demus, D., Goodby, J. W., Gray, G. W., Spiess, H. W., Vill, V., Eds.; Wiley VCH: Weinheim, 1998; Vol. *2B*, pp 865−885; (b) Giroud-Godquin, A. M.; Maitlis, P. M. *Angew. Chem., Int. Ed. Engl.* **1991**, *30*, 375−402 and references therein.